Chapter 1
Multimaterial Fibers

Guangming Tao, Ayman F. Abouraddy, Alexander M. Stolyarov and Yoel Fink

Abstract In recent years, new materials processing approaches have emerged that enable the realization of fiber devices with unique photonic, optoelectronic, and acoustic functionalities. At the heart of this achievement is the identification of materials and processing conditions that mitigate surface energy effects, allowing for materials with disparate optical, electronic, and thermo-mechanical properties to be monolithically drawn from a preform into kilometer-long fibers with complex micro- and nano-structured cross-sectional features. We review this nascent but rapidly growing field and highlight future research directions.

1.1 Introduction

Optical fibers have enhanced the quality of life throughout the world and have fundamentally transformed the human condition in both obvious and imperceptible ways. Today, the worldwide delivery of the internet, and most telecommunications, is achieved through optical fibers [1, 2]. Additionally, optical fibers are used in a multitude of medical and industrial applications ranging from noninvasive

G. Tao · A. F. Abouraddy
CREOL, The College of Optics and Photonics, University of Central Florida,
Orlando, FL, USA
e-mail: guangmingtao@gmail.com

A. F. Abouraddy
e-mail: raddy@creol.ucf.edu

A. M. Stolyarov · Y. Fink (✉)
Research Laboratory of Electronics, Massachusetts Institute of Technology,
Cambridge, MA, USA
e-mail: yoel@mit.edu

A. M. Stolyarov
e-mail: sashok@mit.edu

medical surgery [3, 4] to monitoring the structural integrity of bridges and oil pipelines [5, 6], and fiber lasers are finding applications in materials processing and manufacturing [7]. Interestingly, despite the many complex technological applications of optical fibers, the fibers themselves are remarkably simple from the perspective of materials composition. A single material, silica glass, is used to fabricate the majority of optical fibers in use today. While optical fibers have also been made from other glasses or polymers, silica glass remains the dominant material in producing optical fibers.

With the new physics of photonic band gaps (PBG's) [8], a novel class of optical fibers emerged in the mid 1990s, photonic crystal fibers (PCF's) and photonic band gap fibers [9]. These fibers presented a significant step in overcoming perceived limitations of the structures that could be produced by the traditional process of thermal fiber drawing. In fact, the initial proposal for fabricating silica PBG fibers was dismissed as unfeasible by seasoned practitioners [10] even though no new material was combined with silica, only air holes. Nevertheless, the rapid success of PBG fibers has had unexpected consequences for the process of fiber fabrication itself. One such consequence was the introduction of the concept of 'multimaterial fibers' over the past decade. This new class of fibers leverages the capabilities of traditional fiber fabrication, but aims at developing new fiber structures, functionalities, and applications that stem from altering the materials composition of the fiber. An all-encompassing and conclusive definition to this emerging concept is difficult to provide. Here, as in our recent review article on the subject [11], we define multimaterial fibers to be *high-aspect-ratio structures that comprise multiple distinct materials, typically produced by thermal drawing from a macroscopic scaled-up model called a 'preform'*. Materials with different optical, electronic, thermo-mechanical, and acoustic properties have now been incorporated into the fiber form-factor [12]. The set of fabrication approaches developed in this emerging field are enabling new functionalities that are not usually associated with optical fibers. Examples include fibers that produce an electrical signal when light is incident on the fiber external surface [13–15] or when the temperature of the surrounding environment changes [16]; self-monitoring fibers that measure their own structural integrity [17]; flexible, lightweight fiber arrays that can image the surrounding environment [14, 18]; fibers that can emit or detect acoustic signals [19, 20]; and fibers that incorporate microfluidics for actively tuning their optical properties [21, 22]. Fiber drawing is therefore morphing into a fabrication route for producing photonic and optoelectronic fiber devices that may be potentially incorporated or woven into fabrics, thereby endowing them with new and sophisticated functionalities [12].

Along with the evolution of multimaterial fibers come new ways of thinking about the fiber drawing process itself. Through dimensional reduction, nanostructures such as nanowires with few-nanometer diameters and unprecedented lengths have been produced [23–26]. The fiber cladding may be viewed as a crucible for chemical synthesis and the thermal fiber draw as a catalyst for enabling chemical reactions to take place between reactive species placed in the preform [27–29]. Multimaterial fibers are also a new playground for the controllable study of fluid

dynamics in confined space and over a wide range of length scales [30]. These developments have recently led to a scalable, top-down, in-fiber fabrication process capable of producing complex structured particles over an unprecedented range of diameters spanning both micro- and nano-scales [31].

There are two aspects of fiber production that have been appropriated by the emerging field of multimaterial fibers. First, the process typically starts by preparing a macroscopic preform. Since the preform is structured on the centimeter scale, it is straightforward to create a complex transverse cross section with controllable placement of multiple materials. Second, thermal fiber drawing is an inherently scalable manufacturing process, producing kilometers of fiber with accurate control over size and axial uniformity [32]. In order for the fiber to maintain the complex transverse structure of the multimaterial preform and have all the materials to flow together at the same temperature, restrictions are placed on the allowable materials combinations compatible with this fabrication process. There are some exceptions to this overall approach. For example, multimaterial fibers may be produced by starting with a single-material fiber or wire as a scaffold and proceeding with additive manufacturing. This can include approaches such as dip coating on the outer surface of extended fiber lengths [33] or vapor deposition inside hollow enclaves in short lengths of a pre-existing fiber [34].

Multimaterial fiber research is at the crossroads of many disciples, including optics, materials science, device physics, nanotechnology, and fluid dynamics. While this field is still in its initial stages of development, there has been tremendous recent progress. This chapter consequently aims at providing only a brief and selective overview of some of the main achievements based on our definition of multimaterial fibers provided above. We first discuss in Sect. 1.2 some general constraints on the materials that may be codrawn in the same fiber, and in Sect. 1.3 we describe several general approaches that–to date–have been utilized to produce multimaterial preforms. Section 1.4 focuses on multimaterial fiber devices with novel optical functionalities, such as transverse omnidirectional emitting fiber lasers. In Sect. 1.5 we describe multimaterial fibers endowed with sophisticated electronic, optoelectronic, and even piezoelectric functionalities, in addition to recent work on producing fibers with traditional crystalline semiconductor cores, such as silicon. In the Sect. 1.6, we highlight novel approaches that utilize fiber drawing as a route to synthesize new chemical compounds. We end the chapter by describing some alternative fabrication approaches (Sect. 1.7) and future possibilities (Sect. 1.8).

1.2 Material Constraints and Fiber Drawing

The preform-to-fiber approach for producing optical fibers relies on thermally drawing the fiber from a macroscopic preform in a fiber draw tower [35]. By feeding the preform into a furnace that softens the material, the molten gob at the preform tip is 'pulled' by gravity or an external force and is stretched into a thin fiber strand, after which polymer coatings are added to the fiber surface for

mechanical protection if necessary. Despite the relative simplicity of this fabrication methodology, its efficiency and robustness are behind the thousands of kilometers of optical fiber that span the globe today enabling worldwide communications networks [1, 2]. An alternative approach, the so-called double-crucible method [36], produces optical fibers from glass melts of the core and cladding materials that are pushed through a nozzle. To date, this process has not been used to produce multimaterial fibers.

The transition from traditional single-material fibers to multimaterial fibers dictates materials constraints that stem from the nature of the preform-to-fiber process. In the case of a single-material preform, the parameters of the draw (e.g., the drawing speed) are determined by the material viscosity at the drawing temperature. On the other hand, since multimaterial preforms may contain materials that are incompatible with thermal drawing when taken separately, such as crystalline semiconductors or metals, thermal drawing imposes some constraints on the materials combinations that are compatible with this fabrication strategy. One may gain insight into the feasibility of various materials combinations by examining the viscosity of silica glass, silicon, and gold as a function of temperature, presented in Fig. 1.1a. These materials represent three distinct classes from the perspective of electronic properties: an amorphous insulator, a crystalline semiconductor, and a metal, respectively. Additionally, these three materials have different optical and mechanical properties. Silica is amenable to thermal drawing over a broad range of conditions since its softening temperature ranges from 1400 to 2350 °C. On the other hand, crystalline materials such as silicon and gold are characterized by an abrupt drop in viscosity above the melting temperature T_m where a phase transition takes place. While this physical feature excludes the use of thermal drawing to produce a fiber from a single-material preform made of silicon or gold, nevertheless a multimaterial-preform approach enables the use of such materials in fiber drawing. By making use of a crystalline material such as silicon or gold as a 'core' embedded in an amorphous 'cladding' such as silica, this multimaterial preform may be thermally drawn above the core T_m. In this scenario, the cladding (silica) acts as a supporting scaffold that contains and restricts the flow of the low-viscosity core material (silicon or gold).

This example enables us to outline some general constraints on the construction of multimaterial preforms and the ensuing thermal drawing conditions. First, at least one material should be amorphous and resist devitrification during thermal drawing, typically a glass or polymer. This amorphous 'backbone' material constitutes an outer cladding that supports the other materials during the draw process, thereby maintaining the fiber cross-sectional structure. The amorphous material constituents must be chosen to have overlapping softening temperatures, while the crystalline constituents must have T_m below the drawing temperature. The drawing temperature must be lower than the boiling temperature of the core material. Additionally, care must be taken to avoid fluid instabilities that may occur when the viscosity of the materials is lowered and the transverse dimensions reduced from preform to fiber (see [23, 24, 30, 31] for further details on this issue). Finally, the materials should also have relatively similar thermal expansion coefficients in
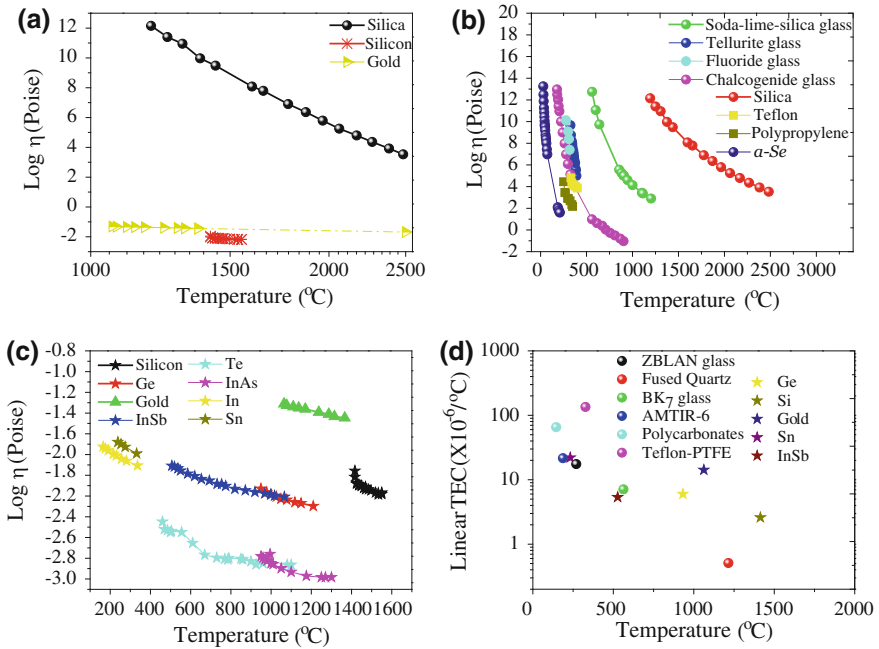
Fig. 1.1 Dynamic viscosity (logarithm of viscosity η in poise) of selected materials versus temperature. **a** Viscosity for silica [37], silicon [38] and gold [39]. The viscosity for silicon and gold are measured above their melting temperatures. **b** Same as (**a**), showing the viscosity for silica [37], soda-lime-silica glass [40], fluoride glass [41], tellurite glass [42], chalcogenide glass (As_2S_3) [43], Teflon®PTFE-6 polymer [44], polypropylene (PP) polymer [45], and amorphous selenium [46]. **c** Same as (**a**), showing the viscosity for silicon [38], germanium [47], indium antimonide [48], tellurium [47], indium arsenide [47], indium [49], tin [49], and gold [39]. **d** Linear thermal expansion coefficient (TEC) at room temperature for selected materials plotted against the melting temperature (T_m) for metals and semiconductors (*solid stars*) and the glass transition temperature (T_g) for the amorphous materials (*solid dots*). References: Ge: T_m [50], TEC [51]; Si: T_m [50], TEC [52]; Gold: T_m [53], TEC [52]; Sn: T_m [53], TEC [54]; InSb: T_m [55], TEC [56]; Teflon® PTFE: T_g [57]; TEC [58]; Fused quartz: T_g [58], TEC [59]; BK7 glass: T_g [58], TEC [58]; AMTIR-6: T_g [60], TEC [60]; Polycarbonates: T_g [61], TEC [59]; ZBLAN glass: T_g [58], TEC [59]

the temperature range extending to the drawing temperature, to avoid fractures resulting from thermo-mechanical mismatches.

The wide range of possibilities for constructing multimaterial preforms within the above-prescribed constraints may be appreciated from Fig. 1.1b where we present the viscosity of a wide range of *amorphous* materials. While some glasses, such as soda-lime-silica, have a broad temperature range suitable for thermal drawing, others (such as fluorides, chalcogenides, and tellurites) have a relatively narrower temperature window. Next, we plot in Fig. 1.1c the viscosity of some typical *crystalline* materials above their T_m. It is possible to choose potential pairs of amorphous-crystalline materials that may be combined in a preform and co-drawn into a multimaterial fiber by consulting Fig. 1.1b, c together. For example, it is

possible to draw a fiber containing a core of Si, Ge, or gold by using a cladding made of silica glass; InSb clad with soda-lime-silica glass glass; or Sn or Se clad with fluoride or chalcogenide glass, or even a polymer. Furthermore, we identify in Fig. 1.1d the glass transition temperature T_g of the amorphous materials and the melting temperature T_m of crystalline materials used in Fig. 1.1a–c versus the linear thermal expansion coefficient (TEC) for completeness. Finally, we note that it is possible for more than two materials to be chosen according to the above criteria and thus be incorporated in the same multimaterial fiber. Indeed, this important possibility enables the construction of in-fiber photonic, electronic and, optoelectronic devices, as described in Sects. 1.4 and 1.5.
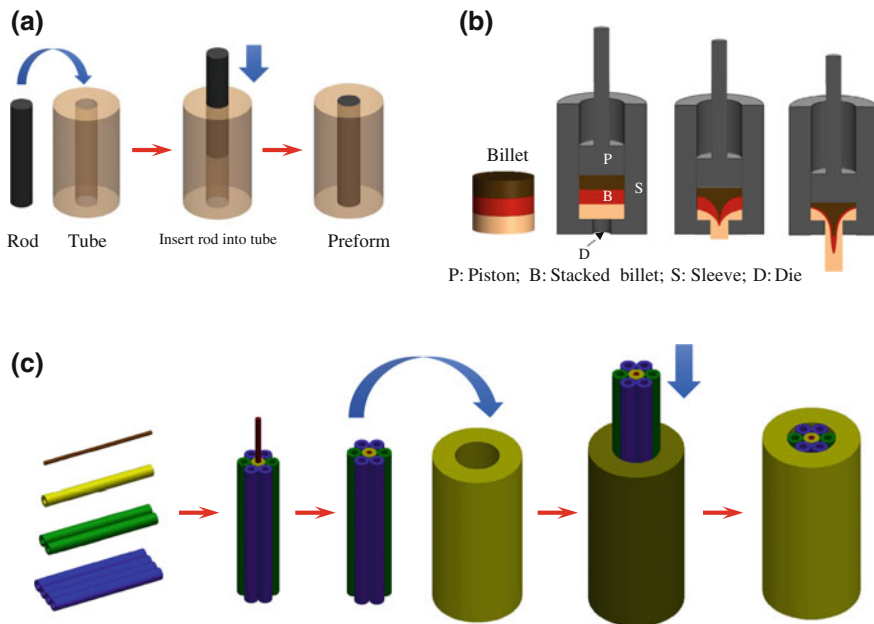
1.3 Multimaterial Preform Fabrication

We describe here four general classes of approaches to the preparation of multimaterial preforms: (a) the rod-in-tube approach [62–64], (b) extrusion [65–67], (c) the stack-and-draw approach [9, 68], and (d) thin-film-rolling technology [12]. The choice of any specific approach, or combinations thereof, is dictated both by the various materials involved and the transverse structure targeted.

1.3.1 Rod-in-Tube Approach

The rod-in-tube approach, depicted in Fig. 1.2a, relies on inserting a solid rod of one material (the core) into a tube of another material (the cladding) to form a preform with a core-cladding structure. In a variation on this procedure, the solid core rod may be replaced with a powder that is placed in the tube. The preform is then sealed and thermally drawn. If T_m of the core powder is lower than the drawing temperature, we designate the process molten-core-in-tube method, a process that enables a wide range of materials to be incorporated as a core. The recognition of the usefulness of this method for multimaterial fibers may be traced back to the pioneering work of E. Snitzer in 1989 [69], where selective volatization combined with the rod-in-tube method was used to produce a silica-clad fiber containing a soft-glass core.

1.3.2 Extrusion

Extrusion is a well-known process used to create axially symmetric objects with a fixed complex cross-sectional profile by 'pushing' a soft material through a die under pressure. The first extrusion process was patented by J. Bramah in 1802 for producing lead pipes [70]. Subsequently, E. Roeder [71–73] extended this approach to soda-lime

(a)

Rod   Tube   Insert rod into tube   Preform

(b)

Billet

P: Piston; B: Stacked billet; S: Sleeve; D: Die

(c)

Fig. 1.2 General methodologies for multimaterial fiber preform fabrication. **a** Rod-in-tube, **b** extrusion, and **c** stack-and-draw methods

silica, lead silicate, calcium aluminate and boric oxide glass in the 1970s. Extrusion makes use of material in the form of a rod, typically called a *billet*, which is placed in a sleeve held inside a furnace (a vertically stacked billet is shown in Fig. 1.2b for illustration). By heating the billet to the softening temperature of the incorporated materials, applied pressure pushes the material through a die that imparts shape to the extruded rod, which may constitute a preform that is subsequently drawn into a fiber. Using a multimaterial billet consisting, for example, of vertically stacked discs, the transverse structure of the extruded rod may be rationally engineered [65, 67].

1.3.3 Stack-and-Draw Approach

An alternative procedure that has been used extensively in preparing the preforms drawn into microstructured fibers, PCFs, and PBG fibers [9] is the stack-and-draw approach. It is instructive that the first prescient demonstration of the stack-and-draw method to produce an optical fiber may be traced to Bell Labs in 1974 [74], at the dawn of the development of silica fibers. In that effort, a fiber containing a hanging core surrounded by air was produced. This procedure offers flexibility in the choice of geometry of the domains for each material by starting from rods, tubes, and/or plates from a single or multiple materials that are assembled into a preform–Fig. 1.2c–with dimensions determined by the targeted fiber structure.

Furthermore, recursive application of multiple stack-and-draw steps enables one to reach the required dimensions (that may not be achievable in a single thermal-drawing step) and attain complex transverse structures.

1.3.4 Thin-Film Rolling

Any of the above three approaches may be used to incorporate polymers into a multimaterial preform. Additionally, a unique process exists to incorporate a polymer in a preform made possible by the availability of polymers in the form of extended thin films. In this technique, a thin polymer film is 'rolled' around a pre-existing rod, followed by thermal consolidation under vacuum above the glass transition temperature of the constituent materials until the individual films fuse. Figure 1.3a details the fabrication approach towards making a multimaterial PBG fiber [75–79], thereby illustrating schematically a particular instance of this process. The thin-film-rolling technique has also been used recursively to realize preforms with complex cross-sections through multiple processing steps. For example, after consolidating a preform constructed in this fashion, voids or enclaves may be introduced that can be filled, for example, by conductors and encapsulated in the preform, followed by rolling additional thin films and reconsolidation. These multistep preform preparation processes form the basis for many recently developed photonic and optoelectronic multimaterial fiber devices [12, 18, 21, 22].

1.4 Photonic Multimaterial Fibers

This section provides an overview of multimaterial fibers with both axial and transverse optical functionality.

1.4.1 Multimaterial PBG Fibers

The MIT fiber group led by Y. Fink demonstrated the first successful draw of multimaterial PBG optical fibers with a hollow core and an all-solid cladding [75]. This was made possible by combining and co-drawing two materials having a large refractive-index contrast, yet compatible thermomechanical properties. Below we describe this and several other examples of photonic multimaterial fiber devices.
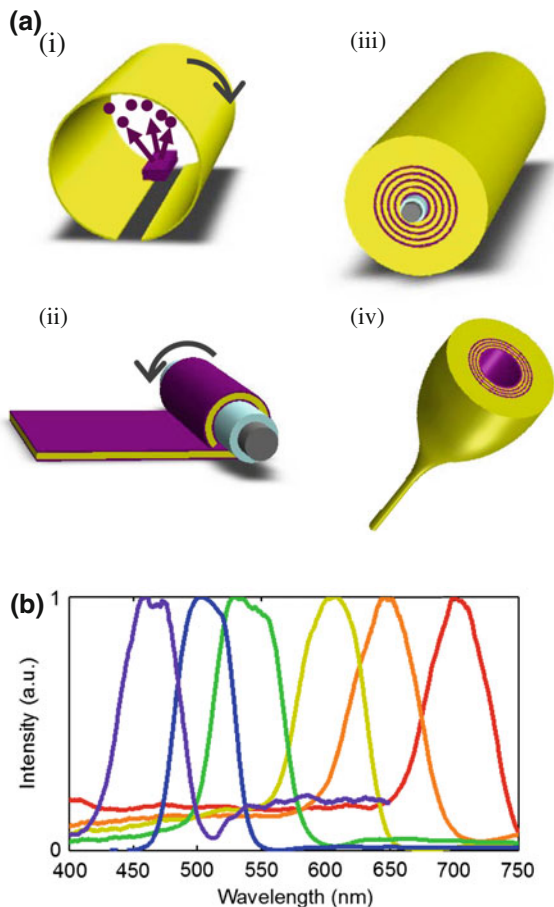
Fig. 1.3 PBG fiber fabrication and characterization **a** PBG fiber fabrication flow. (*i*) The chalcogenide glass is thermally evaporated onto both sides of the polymer film. (*ii*) This multilayer film is then rolled onto a Teflon-lined mandrel and additional polymer cladding layers are rolled for mechanical support. (*iii*) The entire structure is thermally consolidated under vacuum until the materials fuse together into one solid preform. (*iv*) The preform is then thermally drawn into 100 m of fiber by applying uniaxial tension. The ratio of the preform down-feed speed and fiber draw speed dictates the final layer thicknesses. **b** Transmission band gap spectra for hollow-core PBG fibers. The fiber structure in each case is the same. The only difference is that the length of the period in the multilayer structure lining the hollow core is reduced (from *right to left*) resulting in the shift of the transmission PBG spectrum

1.4.1.1 Hollow-Core PBG Fibers

A one-dimensional (1D) periodic stack of alternating high- and low- refractive index materials with a sufficiently large refractive-index contrast can be used to construct an omnidirectional mirror [80, 81], one that reflects light incident at any

angle and polarization within a given spectral window. If this type of a mirror lines the inner surface of a hollow-core fiber, light can be guided axially through the air core [82]. Ideas surrounding such a light-guiding mechanism were considered in the 1970s [83], but it was only in 2002 that the standard preform-to-fiber drawing technique was used to fabricate a multimaterial hollow-core fiber, which realized the first waveguide of this type [75]. The challenge in fabricating these types of multimaterial fibers lies in discovering (or creating) two different thermally compatible materials as well as maintaining the geometric structure during the fiber drawing process. Specifically, the alternating materials must have compatible thermomechanical properties (such that their viscosities overlap at the drawing temperature), and simultaneously they must have a high refractive-index contrast. Furthermore, in order to create a low-loss fiber, the multilayer structure needs to be maintained with low-scattering interfaces down to the micro- and nanoscale. To date, several pairs of materials have been identified which yield low-loss multimaterial optical transmission fibers under appropriate fabrication conditions. Typically, the pair consists of a low-refractive-index polymer and a high-refractive-index chalcogenide glass, which are both amorphous and thermomechanically compatible for fiber drawing [75–77]. The fabrication process for creating hollow-core multimaterial fibers with PBG's is outlined in Fig. 1.3a. The same technique can be used to produce fibers that guide light from the infrared down to ultraviolet. Precise control over the layer thicknesses at the nanometer scale is confirmed by the measured transmission spectra spanning the visible range; see Fig. 1.3b. During the thermal draw, simply increasing the draw speed leads to cross-sectional feature reduction and consequently blue-shifting of the PBG. Such hollow-core, multimaterial PBG fibers have been used in a variety of applications which we describe below

(1) A multiplicity of eigenmodes is supported by the fibers [84] [85]. The ability to precisely excite, propagate, and reconstruct specific fiber modes and their superpositions [78, 86, 87] provides a means to sculpt and tune the vectorial field distribution along the axis of the fiber. These capabilities are particularly interesting for the study of light-matter interaction over extended lengths. Moreover, as the core size decreases, the spiral nature of the multilayer structure— arising from the fabrication approach in Fig. 1.3a—imparts unique properties to the optical modes, such as asymmetric wave propagation [88].

(2) Numerous medical and industrial applications rely on the delivery of high-peak-power laser pulses in well-controlled spatial modes. However, the use of traditional solid-core fibers for handling high peak powers is limited due to material absorption, which sets the damage threshold limit. Multimaterial hollow-core PBG fibers have been shown to transmit peak powers of 11.4 MW at 1.55 μm with 97 % of the fiber output in the fundamental mode, a record for any fiber at this wavelength. Additionally, PBG fibers designed for the transmission of high-power continuous-wave CO_2 laser light at 10.6 μm are used as optical scalpels in minimally invasive medical procedures [75, 89].

(3) Chemical vapor sensing constitutes another application for hollow-core PBG fibers [79, 90]. For example, a chemiluminescent dye that emits light in reaction with peroxide vapor can be introduced into the fiber core. In this way, the fiber provides confinement for the analyte flow and simultaneously serves as an optical waveguide for transmitting the chemiluminescent signal to an optical detector mounted at the distal fiber end [79].

(4) Hollow-core PBG fibers can be used as refractive index sensors since the transmission bandgap spectral position and linewidth change with varying core refractive indices [91, 92].

1.4.1.2 Radial Lasing and Azimuthal Intensity Control

The hollow core of a multimaterial PBG fiber can host a gain medium, enabling the creation of radially emitting fiber lasers [22, 93]. This laser design stands in clear contrast to all other fiber lasers, which emit light axially from their end facet. Two configurations of radially emitting fiber lasers have been explored thus far. One such configuration incorporates an organic dye dissolved in a solid host while another makes use of a liquid host. In both cases, the gain medium plug is introduced in the fiber core and is pumped axially as shown in Fig. 1.4a. In the radial fiber laser architecture, the multilayer structure plays a dual role. The reflection at glancing incidence angles delivers the pump beam to the gain medium plug. The reflection at normal incidence to the fiber reflects the fluorescence back into the core. This radial feedback facilitates laser action in the transverse plane. As shown in Fig. 1.4a, the radiation pattern emitted by the solid plug is anisotropic (with directionality dictated by the pump beam polarization), while the emission from the liquid is rotationally symmetric. This contrast arises from the differences in the relaxation dynamics of excited molecules in the solid and liquid phases.

The rotational symmetry and specific polarization of the radially emitting liquid laser forms the basis for a fiber device with controllable directional emission [22]. Multiple electrically controllable and individually addressable liquid-crystal-based light modulators [22] can be integrated in an annular fashion around the laser cavity, as shown in Fig. 1.4b. Each of the liquid-crystal-filled channels serves to modulate the polarized wavefront emanating from the fiber core and passing through it as it exits the fiber. By controlling multiple microchannels simultaneously, a laser with a dynamically controlled intensity distribution spanning the full azimuthal angular range can be achieved. Figure 1.4c depicts the laser intensity control through one of the channels as a function of the applied voltage. This new capability, implemented monolithically within a single fiber, presents opportunities ranging from flexible multidirectional displays to minimally invasive directed light delivery systems for medical applications.
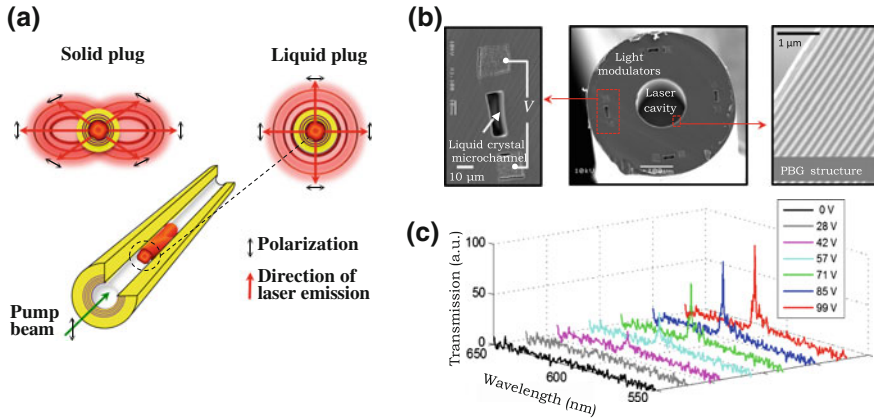
Fig. 1.4 Radial fiber lasers (**a**, *center*) Schematic of a radially emitting fiber laser. The *red cylinder* in the core corresponds to an organic-dye doped plug, which can be a liquid or a solid. (**a**, *left*) Emission patterns from the solid plug and (**a**, *right*) a liquid plug. The *red arrows* denote the direction of laser emission. The direction of the lobes for the solid plug is orthogonal to the pump beam polarization. **b** Scanning electron micrograph of the hybrid fiber containing a cylindrical PBG structure encircled by four hollow microchannels, each flanked by a pair of conductive electrodes. **c** Laser spectra measured for light transmitted through one of the liquid-crystal-filled channels for various driving voltages

1.4.1.3 External Reflection Fibers

Instead of lining the hollow core, the multilayer structure can be introduced at the external surface of the fiber, thereby creating omnidirectional externally reflective fibers [94]. While a purely periodic structure leads to PBG's that reflect light over a broad wavelength range, the intentional deviation from periodicity by introducing a defect layer facilities the existence of localized modes, which leads to narrow band transmission dips within the PBG [8]. These narrowband cavity resonances can be tuned dynamically either by applying an axial strain to the fiber [95] or by optically modulating the defect layer via a transient photodarkening effect [96]. Incorporated into fabrics, such fibers could be used for spectral identification, as radiation barriers, or as large-area tunable optical filters.

1.5 Optoelectronic Fibers

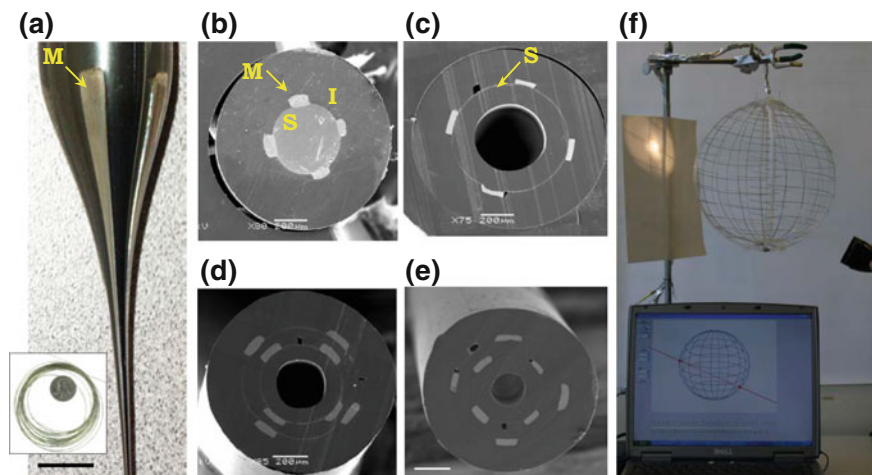### 1.5.1 Metal- Insulator-Semiconductor Fibers

The creation of electronic and optoelectonic devices requires the assembly of metals (M), insulators (I), and semiconductors (S), in prescribed geometries with low-scattering interfaces and nanoscale feature sizes. While traditional wafer-based

approaches have been applied to this problem, they are limited to primarily rigid and low-aspect ratios structures. However, if all the constituent device components could be integrated into a fiber, the complex functionality associated with modern-day chip-based devices could extend into the fabrics that we wear.

While the insulating and semiconducting domains can both be amorphous and thus can be drawn in a highly viscous state, a particular challenge involves the incorporation of a crystalline metallic domain into the fiber. Since the metal undergoes a phase transition into the liquid state during the draw, it is susceptible to capillary breakup and can easily disrupt the structural integrity of the fiber. These challenges can be addressed by confining the metallic electrodes within highly viscous boundaries, which can help to suppress capillary instabilities and direct the flow of the metal during the draw. Several M–I–S fiber structures have been created thus far using this approach. Figure 1.5a depicts a M–I–S preform being elongated into a fiber and the corresponding scanning electron microscope (SEM) image of the cross section is shown in Fig. 1.5b [15]. The core of the fiber is an amorphous photoconductive semiconductor (a semiconducting chalcogenide glass). The electrodes which contact the semiconductor can be connected to an external circuit post draw, and this fiber can then be used as a photodetector, which produces a photocurrent signal in proportion to the optical power incident onto its surface. Two advantages are gained by reducing the bulk semiconductor cylinder to a thin-film structure such as shown in Fig. 1.5c [13]. First, the dark current, which sets the noise level for optoelectronic applications, is reduced by more than an order of magnitude. Second, the creation of thin-film structures enables higher device-density per fiber (Fig. 1.5d) as well as the creation of more elaborate geometries (Fig. 1.5e) [18]. All of these structures are axially symmetric, with the electrodes forming intimate contacts with the semiconducting chalcogenide glass layers along the entire fiber length.

Both the composition of the semiconducting chalcogenide glass and the geometry of other structural elements comprising the preform can be tuned to target particular applications.

(1) By using a photoconductive glass, photodetecting fibers are created with the ability of detecting illumination along their entire length [13, 15, 18, 97], which has applications spanning chemical vapor sensing [98] to lensless imaging [14, 18]. Each pair of adjacent electrodes can act as an independent photodetector, thereby imparting increasing functionality. For example, a semiconductor ring structure (Fig. 1.5c) can be used to determine the angle of incidence of an incoming beam in the plane perpendicular to the fiber axis. Moreover, the semiconductor's wavelength-dependent absorbance may be leveraged using a duel ring structure (Fig. 1.5d) to reconstruct the wavelength of an incident beam by measuring the ratio of photocurrents in the inner and outer rings.

(2) Photoconductive glasses typically respond over a broad wavelength range. In order to impart spectral selection to a photosensitive fiber, a multilayer reflector containing a defect cavity can be combined with a photodetecting

Fig. 1.5 Metal (*M*)—Insulator (*I*)—Semiconductor (*S*) Fibers **a** Picture of an M-I–S preform scaling down into a fiber. (Scale bar is 1 cm). Inset shows several meters of coiled fiber. **b–e** SEM micrographs of various M-I–S fiber architectures. (Scale bar for **b**, **c**, **d**, **e**: 200, 200, 200, 100 μm). **f** A spherical fiber web is an omnidirectional photodetector which can detect the direction on an optical beam incident from any angle. The reconstructed path of the flashlight beam passing through the sphere is seen on the computer monitor

structure [15]. The thickness of the defect cavity determines the narrowband transmission window within the PBG, allowing the engineering of spectroscopic photosensitive fibers tuned to respond at specific wavelengths.

(3) A semiconductor with a temperature-dependent resistivity can be drawn into a fiber with the identical geometry as shown in Fig. 1.5b, but with the ability to detect changes in temperature along its entire length [16]. Integrated into fabrics, such fibers can be used for temperature sensing over large areas. Moreover, a thin film ring of the same semiconductor can be integrated into a PBG transmission fiber to predict the onset of fiber failure [17].

(4) The electronic properties of the semiconductor can also be significantly improved through crystallization post-draw. This method has been used for realizing in-fiber field-effect transistors [99] and rewritable memory devices reminiscent of the ovonic switches [100].

Meters of fiber result from a single draw, thus facilitating the construction of large area assemblies and fabrics with optoelectronic, thermal, and acoustic functionalities. For example, a transparent sphere made of photodetecting fibers (Fig. 1.5f) can reconstruct the direction of an optical beam incident from any angle. Furthermore, the wavelength-reconstruction property of the dual-ring fiber structures (Fig. 1.5d) enable a two-dimensional fiber grid to perform lensless imaging [18], thus opening the possibility for fabrics that can *see*.

In addition to optoelectronic functionality, multimaterial fibers can be endowed with acoustic functionality through the piezoelectric effect. This can be achieved by drawing a copolymer, P(VDF- TrFE), that has a stable beta-phase at room temperature, and therefore will directly crystallize from the melt into the piezoelectric phase. Rectangular and cylindrical piezoelectric fibers have been drawn, both with the capability to emit and detect acoustic radiation over a broad frequency range spanning the kHz to MHz [19]. The ability to change the fiber cross-sectional geometry is particularly interesting for piezoelectric fibers, as this provides the means to tune the acoustic radiation pattern emanating from the fiber. Arrays of piezoelectric fibers can thus be constructed, leading to sophisticated functionalities such as coherent acoustic wave interference and beam steering [20], and large-area acoustic fiber webs can pave the way towards novel applications ranging from large-area pressure-wave monitoring to communications.

1.5.2 Crystalline-Semiconductor-Core Fibers

The mainstay of the microelectronic industry is crystalline semiconductors such as silicon (Si) and germanium (Ge), which have superior electronic properties compared to amorphous semiconductors. Therefore, to expand the performance of in-fiber electronic devices, there is a growing interest in developing methods to thermally draw these more traditional semiconductor materials. The optical properties of Si and Ge are also attractive: they are transparent in the midinfrared, have high optical damage threshold [101, 102], and are also highly nonlinear [103, 104]. For example, the Raman gain coefficient in Si is $\sim 10^4$ times greater than that of silica. Furthermore, the high thermal conductivity of Si and Ge offers opportunities in better removal of dissipated heat. The extension from planar substrates to optical fibers [34, 62] is therefore a significant complement to the emerging field of silicon photonics [105–108].

There has been significant recent progress in developing fibers containing traditional crystalline semiconductors. The first thermally drawn Si-core optical fiber was demonstrated using the molten-rod-in-tube method by J. Ballato's group in 2008 [62] (Fig. 1.6a). The melting temperature of Si (~ 1416 °C) overlaps with the softening temperature of silica (Fig. 1.1a); therefore, this materials combination in a multimaterial fiber is feasible from a thermal compatibility standpoint. A Si rod (3 mm diameter, 40 mm length) is inserted into a thick-walled silica tube, and the assembled preform is drawn into tens of meters of fiber with core diameters of approximately 60–120 μm. This approach has been extended to several other semiconductors such as Ge [109, 110] (Fig. 1.6b) and InSb [111], as well as to more complex materials systems, such as sapphire-derived high-alumina-content optical fibres [112].

Although this fiber is extremely simple from an elemental-analysis perspective (Si and O are the only two elements involved), this glass/crystalline-semiconductor materials system has nevertheless proven very fruitful in fundamental studies of
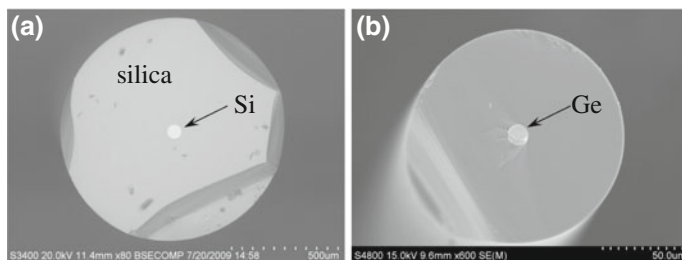
Fig. 1.6 Crystalline semiconductor core fibers. **a** Scanning electron micrograph of the core region of the silicon core, silica-clad optical fiber in [62]. **b** Electron micrographs of a crystalline Ge core optical fiber from [109]

diffusion and crystallization in confined volumes. Extensive work by J. Ballato's group, using X-ray diffraction, Raman spectroscopy, and spatially resolved crystallographic orientation studies [110, 113], have elucidated the polycrystalline domain structure of the core along the fiber. Several approaches have been exploited to increase the axial length of the single-crystal domains, including fiber-annealing by rapid photothermal processing (RPP) and controlling the core geometry [114], which have led to larger single-crystal domains. It is expected that such approaches will yield fibers with improved structural, electrical, optical, and mechanical properties.

Another research effort to produce Si-core fibers using the powder-in-tube method is reported in [63]. Silicon powder is packed into a silica tube which is then evacuated in order to limit the oxidation of Si. Outer diameters in the range of several hundred microns and core diameters in the range of tens of microns of n-type Si optical fibers have been demonstrated by this method [63]. High optical losses have been observed, which are attributed to irregularities along the fiber, such as thermal-expansion-induced micro-cracks at the core/cladding boundary and the polycrystallinity of the Si core.

This area of research is expected to blossom in the next few years with more research groups entering this field. While the focus to date has been on the materials science aspect of this class of multimaterial fibers, it is anticipated that the maturation of this field will lead to the development of fibers endowed with electronic and optoelectronic functionalities having potential applications in functional clothing and solar energy harvesting.

1.6 In-Fiber Synthesis

A recent surprising development in multimaterial fibers has resulted from the observation that the high-temperatures associated with thermal fiber drawing combined with the potential of using core and cladding materials with very

different chemical reactivity offer the possibility of exploiting fiber drawing in *chemical synthesis*. On this view, the preform cladding acts as a crucible in which a chemical synthesis process is confined in the core. First, physical changes take place during fiber drawing, namely a reduction in the core and cladding viscosity, and potentially melting or volatization of the core, in addition to the geometric constriction of the core material(s). Crucially, in the in-fiber synthesis approach, such *physical* changes are then accompanied by *chemical* changes. For example, new compounds may be produced in the core, either via reactions between pre-existing core compounds, or through diffusion of elements or compounds from the cladding into the core. This methodology constitutes one example of a re-imagining of the fiber drawing process itself, where the elongation at high temperature of multimaterial fibers is used to achieve a new goal: controlled chemical reactions along an extended length in a precisely controlled, confined geometry.

The concept of multimaterial in-fiber synthesis may be traced back to the work by E. Snitzer and R. Tumminelli in 1989 [69] (see Sect. 1.3). The fiber drawing temperature in that realization was higher than T_m of the core material (a soft-glass) and its higher vapor pressure in the liquid phase led to the volatization of some compounds in the hot neck-down region resulting in a different residual core composition. This early work may also be viewed as a first instance of co-drawing two families of materials having incompatible thermal properties.

Another example drawn from more recent work demonstrated the possibility of synthesizing a material—whose melting temperature far exceeds the draw temperature—starting from low-temperature precursors. Specifically, low-temperature materials $Se_{97}S_3$ and $Sn_{85}Zn_{15}$ were co-drawn and a ZnSe compound was produced in the drawn fiber [27]. The synthesized compound—ZnSe here—has a much higher melting temperature than the drawing temperature. Additionally, J. Ballato et al. [28] have used crystalline Bi_2O_3-rich ($Bi_2O_3 + GeO_2$) and $Bi_{12}GeO_{20}$ powders (core) placed in borosilicate glass tube (cladding) to produce fibers where an in situ chemical reaction occurs during the thermal drawing in both amorphous and crystalline cores. Furthermore, in an attempt to reduce the diffusion of oxygen from the silica cladding to the Si core, silicon carbide (SiC) was introduced into the core to provide an in situ reactive oxygen getter during the drawing process [115]. This novel processing route can be used potentially to produce fiber cores from materials that are difficult to fabricate or machine into a rod using conventional methods among many other possible applications.

1.7 Other Approaches

In this chapter, we have described various multimaterial fibers that have been produced using the general methodology of preform-to-fiber fabrication. Recently, alternative strategies have emerged that also produce multimaterial fibers but do not rely on first constructing a macroscopic preform. We briefly describe these interesting exceptions in this section for completeness. First, an approach developed by

Konarka, Inc., starts from a long steel wire that is used in successive steps of dip-coating in organic solutions [33] to produce an organic photovoltaic fiber. The resulting fiber formed of a multilayer coating along its whole length constitutes an organic photovoltaic cell that demonstrated ∼3% efficiency. A second approach uses a silica fiber with hollow enclaves (either a hollow-core fiber or a PCF) as a scaffold for vapor deposition of traditional crystalline semiconductors, a process typically called high-pressure microfluidic chemical deposition (HPMCD) [34] that extends the material phases that may be incorporated into the fiber to *single-crystal* semiconductors [116] and polycrystalline elemental or compound semiconductors [111, 117]. This process requires high-pressure flow (2–1000 MPa) in silica microstructured optical fibers (MOF's) to overcome mass-transport constraints, resulting in uniform annular deposition onto hollow pore walls. Two well-developed fabrication methodologies are combined in this approach: chemical vapor deposition (CVD) [118] and silica fiber drawing. The basic idea is shown in Fig. 1.7a, which involves heating small quantities of a high-pressure precursor within the interior of a MOF that decomposes upon heating to deposit on the walls in an amorphous state to ensure that it bonds smoothly, followed by annealing for crystallization. Figure 1.7b is an example of deposited doped semiconductor layers and metals [119]. As the annular deposited film grows thicker, the central holes from which depositions occurs becomes smaller until it is completely plugged and flow is extinguished. The empty pores in the MOFs are thus treated as micro- or nano-scale reaction chambers. A fiber-based device fabricated using this approach enabled all-optical modulation of 1.55 μm guided light via free-carrier absorption mediated by a 532 nm pump pulse [120]. Other examples include producing a ZnSe-core fiber [117], in-fiber Si and Ge wires and tubes used as field effect transistors [121], and in-fiber crystalline Si p–n homojunctions and Pt/n-Si Schottky heterojunctions [119]. The HPCVD technique can accommodate different capillary core dimensions and may also be used to fill a large number of micro- and nano-scale pores in MOF's. The main drawback of this technology is the limited lengths of fiber devices produced compared to those resulting from fiber drawing.

1.8 Conclusions and Outlook

We have presented an outline of the wide range of exciting ideas currently under active investigation in the emerging field of multimaterial fibers. Over the past decade, this field has witnessed rapid growth and it is impossible to cover all the ideas being explored in this chapter. For example, we did not describe interesting new work on producing THz multimaterial-fiber metamaterials [122–126]. Metamaterials are synthetic photonic structures that may potentially enable exotic optical phenomena such as 'cloaking' [127]. Some of the necessary features of a metamaterial, such as control over the electrical and magnetic resonances experienced by THz radiation transmitted through the transverse fiber cross sections, have been observed using polymer fibers containing arrays of metallic structures.
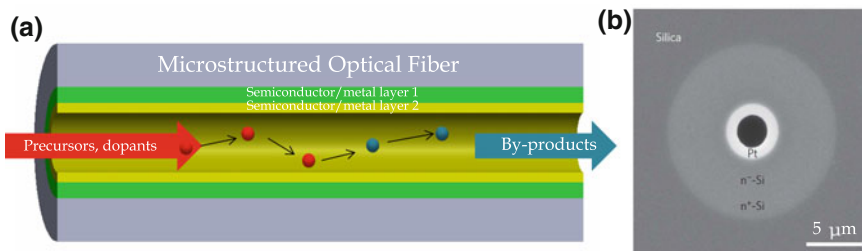
Fig. 1.7 Integration of semiconductor junctions in MOFs. **a** Illustration of HPCVD in a MOF pore. **b** A Pt/n$^-$-Si Schottky junction formed by sequential deposition of phosphorous doped n$^+$-Si, n$^-$-Si and platinum layers [119]

Extending this approach to optical wavelengths will require further reduction of the feature sizes in the multimaterial fibers. Other examples include the use of gold in silica fibers for plasmonic studies [128–133], the use of polymers to produce robust infrared chalcogenide fibers and nano-tapers [67, 134, 135], and the use of soft glasses inside silica fibers for mid-infrared nonlinear applications [136, 137].

An important avenue for further research is increasing the density of optical, electronic and optoelectronic devices incorporated in a single multimaterial fiber. Another opportunity is the production of fibers endowed with such functionalities in a form that may be directly woven into fabrics, which would constitute a milestone for this field, leading to a marriage of optics, electronics, and textiles. Another recent avenue has focused on using in-fiber capillary instabilities to produce three-dimensional macroscopic synthetic photonic structures with nanoscale control over the material distribution [30, 31], which may enable unprecedented control over the behavior of light and sound. A recent example of this can be found in [138] where the ability to produce in-fiber, electrically rectifying p-n composite micro-particles from the controlled fluidic breakup of two adjacent p- and n-doped silicon cores embedded in a silica cladding was demonstrated. Many surprises, no doubt, lie ahead, and it is thus safe to predict that the progress in multimaterial fibers reviewed here is pointing to a renaissance in fiber fabrication that promises to continue for a long time to come.

References

1. G.P. Agrawal, *Fiber-Optic Communication Systems*, 4th edn. (Wiley, Hoboken, 2010)
2. R. Ramaswami, K.N. Sivarajan, G.H. Sasaki, *Optical Networks: A Practical Perspective*, 3rd edn. (Morgan Kaufmann Publishers Inc., San Francisco, 2009)
3. J.I. Peterson, G.G. Vurek, Fiber-optic sensors for biomedical applications. Science **13**(224), 123–127 (1984)
4. A.G. Mignani, F. Baldini, Biomedical sensors using optical fibres. Rep. Prog. Phys. **59**, 1–28 (1996)
5. Z. Zhou, J. He, M. Huang, J. He, and G. Chen, Casing Pipe Damage Detection with Optical Fiber Sensors: A Case Study in Oil Well Constructions, Adv. Civil Eng. 638967, 9 (2010)
6. N. Mohamed, I. Jawhar, J. Al-Jaroodi, L. Zhang, Sensor network architectures for monitoring underwater pipelines. Sensors **11**(11), 10738–10764 (2011)
7. T. Webber, in *Advances in Fiber Lasers for the Materials Processing Market, Quantum Electronics and Laser Science Conference (QELS) on Advances in High-Power Lasers and their Applications III: Processing (JTh4I)*, San Jose, California, USA, 6 May 2012
8. J.D. Joannopoulos, S.G. Johnson, J.N. Winn, R.D. Meade, *Photonic Crystals. Molding the Flow of Light*, 2nd edn. (Princeton University Press, Princeton, 2008)
9. P. Russell, Photonic crystal fibers. Science **299**, 358–362 (2003)
10. P. Russell, Photonic crystal fibers: a historical account. IEEE LEOS Newsletters **21**(5), 11–15 (2007)
11. G. Tao, A.M. Stolyarov, A.F. Abouraddy, Multimaterial fibers. I. J. Appl. Glass Sci. **3**(4), 349–368 (2012)
12. A.F. Abouraddy, M. Bayindir, G. Benoit, S.D. Hart, K. Kuriki, N. Orf, O. Shapira, F. Sorin, B. Temelkuran, Y. Fink, Towards multimaterial multifunctional fibres that see, hear, sense and communicate. Nat. Mater. **6**, 336–347 (2007)
13. F. Sorin, A.F. Abouraddy, N. Orf, O. Shapira, J. Viens, J. Arnold, J.D. Joannopoulos, Y. Fink, Multimaterial photo detecting fibers: a geometric and structural study. Adv. Mat. **19**, 3872–3877 (2007)
14. A.F. Abouraddy, O. Shapira, M. Bayindir, J. Arnold, F. Sorin, D. Saygin-Hinczewski, J.D. Joannopoulos, Y. Fink, Large-scale optical-field measurements with geometric fibre constructs. Nat. Mater. **5**, 532–536 (2006)
15. M. Bayindir, F. Sorin, S. Hart, O. Shapira, J.D. Joannopoulos, Y. Fink, Metal-insulator-semiconductor optoelectronic fibres. Nature **431**, 826–829 (2004)
16. M. Bayindir, A.F. Abouraddy, J. Arnold, J.D. Joannopoulos, Y. Fink, Thermal-sensing fiber devices by multimaterial codrawing. Adv. Mat. **18**, 845–849 (2006)
17. M. Bayindir, O. Shapira, D. Saygin-Hinczewski, J. Viens, A.F. Abouraddy, J.D. Joannopoulos, Y. Fink, Integrated fibers for self monitored optical transport. Nat. Mater. **4**, 820–824 (2005)
18. F. Sorin, O. Shapira, A.F. Abouraddy, M. Spencer, N.D. Orf, J.D. Joannopoulos, Y. Fink, Exploiting collective effects of multiple optoelectronic devices integrated in a single fiber. Nano Lett. **9**, 2630–2635 (2009)
19. S. Egusa, Z. Wang, N. Chocat, Z.M. Ruff, A.M. Stolyarov, D. Shemuly, F. Sorin, P.T. Rakich, J.D. Joannopoulos, Y. Fink, Multimaterial piezoelectric fibres. Nat. Mater. **9**, 643–648 (2010)
20. N. Chocat, G. Lestoquoy, Z. Wang, D. M. Rodgers, J. D. Joannopoulos, Y. Fink, Piezoelectric fibers for conformal acoustics, Adv. Mat. doi: 10.1002/adma.201201355. (2012)
21. A.M. Stolyarov, L. Wei, F. Sorin, G. Lestoquoy, J.D. Joannopoulos, Y. Fink, Fabrication and characterization of fibers with built-in liquid crystal channels and electrodes for transverse incident-light modulation. Appl. Phys. Lett. **101**, 011108 (2012)

22. A.M. Stolyarov, L. Wei, O. Shapira, F. Sorin, S.L. Chua, J.D. Joannopoulos, Y. Fink, Microfluidic directional emission control of an azimuthally polarized radial fibre laser. Nat. Photonics **4**, 229–233 (2012)

23. D.S. Deng, N.D. Orf, A.F. Abouraddy, A.M. Stolyarov, J.D. Joannopoulos, H.A. Stone, Y. Fink, In-fiber semiconductor filament arrays. Nano Lett. **8**, 4265–4269 (2008)

24. D.S. Deng, N.D. Orf, S. Danto, A.F. Abouraddy, J.D. Joannopoulos, Y. Fink, Processing and properties of centimeter-long, in-fiber, crystalline-selenium filaments. Appl. Phys. Lett. **96**, 023102 (2010)

25. M. Yaman, T. Khudiyev, E. Ozgur, M. Kanik, O. Aktas, E.O. Ozgur, H. Deniz, E. Korkut, M. Bayindir, Arrays of indefinitely long uniform nanowires and nanotubes. Nat. Mater. **10**, 494–501 (2011)

26. J.J. Kaufman, G. Tao, S. Shabahang, D.S. Deng, Y. Fink, A.F. Abouraddy, Thermal drawing of high-density macroscopic arrays of well-ordered sub-5-nm-diameter nanowires. Nano Lett. **11**, 4768–4773 (2011)

27. N.D. Orf, O. Shapira, F. Sorin, S. Danto, M.A. Baldo, J.D. Joannopoulos, Y. Fink, Fiber draw synthesis. P. Natl. Acad. Sci. USA **108**(12), 4743–4747 (2011)

28. J. Ballato, C. McMillen, T. Hawkins, P. Foy, R. Stolen, R. Rice, L. Zhu, O. Stafsudd, Reactive molten core fabrication of glass-clad amorphous and crystalline oxide optical fibers. Opt. Mater. Express **2**(2), 153–160 (2012)

29. C. Hou, X. Jia, L. Wei, A.M. Stolyarov, O. Shapira, J.D. Joannopoulos, Y. Fink, Direct atomic-level observation and chemical analysis of ZnSe synthesized by in situ high-throughput reactive fiber drawing. Nano Lett. **13**(3), 975–979 (2013)

30. S. Shabahang, J.J. Kaufman, D.S. Deng, A.F. Abouraddy, Observation of the plateau-rayleigh capillary instability in multi-material optical fibers. Appl. Phys. Lett. **99**, 161909 (2011)

31. J.J. Kaufman, G. Tao, S. Shabahang, E.-H. Banaei, D.S. Deng, X. Liang, S.G. Johnson, Y. Fink, A.F. Abouraddy, Structured spheres generated by an in-fibre fluid instability. Nature **487**, 463–467 (2012)

32. M. Bayindir, A.F. Abouraddy, O. Shapira, J. Viens, D. Saygin-Hinczewski, F. Sorin, J. Arnold, J. Joannopoulos, Y. Fink, Kilometer-long ordered nanophotonic devices by preform-to-fiber fabrication. IEEE J. Sel. Top. Quant. **12**(6), 1202–1213 (2006)

33. M.R. Lee, R.D. Eckert, K. Forberich, G. Dennler, C.J. Brabec, R.A. Gaudiana, Solar power wires based on organic photovoltaic materials. Science **324**, 232–235 (2009)

34. P.J.A. Sazio, A. Amezcua-Correa, C.E. Finlayson, J.R. Hayes, T.J. Scheidemantel, N.F. Baril, B.R. Jackson, D.-J. Won, F. Zhang, E.R. Margine, V. Gopalan, V.H. Crespi, J.V. Badding, Microstructured optical fibers as high-pressure microfluidic reactors. Science **311**, 1583–1586 (2006)

35. T. Li (ed.), *Optical fiber communications: fiber fabrication* (Academic Press, Waltham, 1985)

36. H. Tokiwa, Y. Mimura, T. Nakai, O. Shinbori, Fabrication of long single-mode and multimode fluoride glass fibres by the double-crucible technique. Electronics Lett. **21**(24), 1131–1132 (1985)

37. G. Urbain, Y. Bottinga, P. Richet, Viscosity of liquid silica, silicates and alumino-silicates. Geochim. Cosmochim. Acta. **46**, 1061–1072 (1982)

38. K. Kakimoto, M. Eguchi, H. Watanabe, T. Hibiya, Natural and forced convection of molten silicon during czochralski single crystal growth. J. Cryst. Growth **94**(2), 412–420 (1989)

39. D. Ofte, The viscosities of liquid uranium, gold and lead. J. Nucl. Mater. **22**(1), 28–32 (1967)

40. A. Napolitano, E.G. Hawkins, Viscosity of a standard soda-lime-silica glass. J. Res. NBS A Phys. Ch. **68A**(5), 439–448 (1964)

41. M. Braglia, C. Bruschi, D. Cavalli, G. Cocito, D. Guojun, J. Kraus, S. Mosso, Rheology of fluoride glasses. J. Crystal. Solid **213–214**(12), 325–329 (1997)

42. A. Belwalkar, W.Z. Misiolek, J. Toulouse, Viscosity study of the optical tellurite glass: 75TeO$_2$-20ZnO-5Na$_2$O. J. Non-Crystal. Solid **356**(1), 1354–1358 (2010)

43. A.S. Tverjanovich, Temperature dependence of the viscosity of chalcogenide glass-forming melts. Glass Phys. Chem. **29**(6), 532–536 (2003)
44. B. Chu, K. Linliu, Viscosity characterization of poly(tetrafluoroethylene) by centrifuge ball viscosimetry. Macromolecules **28**(8), 2723–2727 (1995)
45. B. Collins, J. Shields, K. Butler, M. Seck, T.J. Ohlemiller, Exploring the Role of Polymer Melt Viscosity in Melt Flow and Flammability Behavior, National Institute of Standards and Technology (BFRL), Gaithersburg, MD., ProductType: Technical report, NTIS Order Number: PB2007-105069, p 29 (2000)
46. P. Koštál, J. Málek, Viscosity of selenium melt. J. Non-Crystal. Solid **356**(50–51), 2803–2806 (2010)
47. V.M. Glazov, S.N. Chizhevskaya, N.N. Glagoleva, *Liquid Semiconductors* (Plenum Press, New York, 1969)
48. Y. Sato, T. Nishizuka, T. Takamizawa, T. Yamamura, Y. Waseda, Viscosity of molten GaSb and InSb. Int. J. Thermophys. **23**, 235–243 (2002)
49. M.F. Culpin, The viscosity of liquid indium and liquid tin. Proc. Phys. Soc. B **70**(11), 1069–1078 (1957)
50. A. Dargys, J. Kundrotas, *Handbook on physical properties of Ge, Si, GaAs and InP* (The Science and Encyclopaedia Publishing Centre, Vilnius, 1994)
51. http://www.owlnet.rice.edu/~msci301/ThermalExpansion.pdf
52. ASM Handbook: Properties and Selection: Nonferrous Alloys and Special-Purpose Materials (ASM Handbook) vol. 2, 10th edn, ASM International, Metals Park, OH, 1990, 704–705 (Au), 1154–1156 (Si)
53. http://www.engineersedge.com/properties_of_metals.htm
54. F.C. Nix, D. MacNair, The thermal expansion of pure metals: copper, gold, aluminum, nickel, and iron. Phys. Rev. **60**, 597–605 (1941)
55. http://www.ioffe.ru/SVA/NSM/Semicond/InSb/thermal.html
56. D.F. Gibbons, Thermal expansion of some crystals with the diamond structure. Phys. Rev. **112**, 136–140 (1958)
57. http://www2.dupont.com/Teflon_Industrial/en_US/tech_info/techinfo_compare.html
58. M.J. Weber, *Optics Handbook of Optical Materials* (CRC PRESS, Boca Raton 2003), section 3.4 (Teflon-PTFE), section 2.4 (fused silica), section 2.2.4 (BK7) and section 2.5.1 (ZBLAN)
59. M. Bass, E.W. Van Stryland, D.R. Williams, W.L. Wolfe, *Handbook of Optics Volume II Devices, Measurements, and Properties*, 2nd edn. (McGraw-Hill INC, New York, 1995), p33.55 (fused Silica and ZBLAN) p7.9 (Polycarbonate)
60. www.amorphousmaterials.com
61. http://www.polymerprocessing.com/polymers/PC.html
62. J. Ballato, T. Hawkins, P. Foy, R. Stolen, B. Kokuoz, M. Ellison, C. McMillen, J. Reppert, A.M. Rao, M. Daw, S.R. Sharma, R. Shori, O. Stafsudd, R.R. Rice, D.R. Powers, *Silicon Optical Fiber*. Opt. Express **16**(23), 18675–18683 (2008)
63. B.L. Scott, K. Wang, G. Pickrell, Fabrication of n-type silicon optical fiber. IEEE Photon. Technol. Lett. **21**(24), 1798–1800 (2009)
64. H.K. Tyagi, H.W. Lee, P. Uebel, M.A. Schmidt, N. Joly, M. Scharrer, P.St.J. Russell, Plasmon Resonances on Gold Nanowires Directly Drawn in a Step-index Fiber, Opt. Lett. **35**(15) 2573–2575 (2010)
65. D.J. Gibson, J.A. Harrington, Extrusion of hollow waveguide preforms with a one-dimensional photonic bandgap structure. J. Appl. Phys. **95**(8), 3895–3900 (2004)
66. X. Feng, T.M. Monro, P. Petropoulos, V. Finazzi, D.J. Richardson, Extruded single-mode high-index-core one-dimensional microstructured optical fiber with high index-contrast for highly nonlinear optical devices. Appl. Phys. Lett. **87**(8), 081110 (2005)
67. G. Tao, S. Shabahang, E.-H. Banaei, J.J. Kaufman, A.F. Abouraddy, Multimaterial preform coextrusion for robust chalcogenide optical fibers and tapers. Opt. Lett. **37**(13), 2751–2753 (2012)

68. M. Liao, C. Chaudhari, G. Qin, X. Yan, C. Kito, T. Suzuki, Y. Ohishi, M. Matsumoto, T. Misumi, Fabrication and characterization of a chalcogenide-tellurite composite microstructure fiber with high nonlinearity. Opt. Express **17**(24), 21608–21614 (2009)
69. E. Snitzer, R. Tumminelli, SiO_2-clad fibers with selectively volatilized soft-glass cores. Opt. Lett. **14**(14), 757–759 (1989)
70. H.L. Blackmore, *A Dictionary of London Gunmakers* (Phaidon—Christie's Limited, Oxford, 1986), p. 59
71. E. Roeder, Extrusion of glass. J. Non-Cryst. Solids **5**(5), 377–388 (1971)
72. E. Roeder, Flow behaviour of glass during extrusion. J. Non-Cryst. Solids **7**(2), 203–220 (1972)
73. W. Egel-Hess, E. Roeder, Extrusion of glass melts-influence of wall friction effects on the die swell phenomenon. Glasstech. Ber. **62**(8), 279–284 (1989)
74. P. Kaiser, H.W. Astle, Low-loss single-material fibers made from pure fused silica. AT&T Tech. J. **53**(6), 1021–1039 (1974)
75. B. Temelkuran, S.D. Hart, G. Benoit, J.D. Joannopoulos, Y. Fink, Wavelength-scalable hollow optical fibres with large photonic bandgaps for co_2 laser transmission. Nature **420**, 650–653 (2002)
76. K. Kuriki, O. Shapira, S. Hart, G. Benoit, Y. Kuriki, J. Viens, M. Bayindir, J. Joannopoulos, Y. Fink, Hollow multilayer photonic bandgap fibers for nir applications. Opt. Express **12**(8), 1510–1517 (2004)
77. Z. Ruff, D. Shemuly, X. Peng, O. Shapira, Z. Wang, Y. Fink, Polymer-composite fibers for transmitting high peak power pulses at 1.55 microns. Opt. Express **18**(15), 15697–15703 (2010)
78. D. Shemuly, A.M. Stolyarov, Z.M. Ruff, L. Wei, Y. Fink, O. Shapira, Preparation and transmission of low-loss azimuthally polarized pure single mode in multimode photonic band gap fibers. Opt. Express **20**(6), 6029–6035 (2012)
79. A.M. Stolyarov, A. Gumennik, W. McDaniel, O. Shapira, B. Schell, F. Sorin, K. Kuriki, G. Benoit, A. Rose, J.D. Joannopoulos, Y. Fink, Enhanced chemiluminescent detection scheme for trace vapor sensing in pneumatically-tuned hollow core photonic bandgap fibers. Opt. Express **20**(11), 12407–12415 (2012)
80. J.N. Winn, Y. Fink, S. Fan, J.D. Joannopoulos, Omnidirectional reflection from a one-dimensional photonic crystal. Opt. Lett. **23**, 1573–1575 (1998)
81. Y. Fink, J.N. Winn, S. Fan, C. Chen, J. Michel, J.D. Joannopoulos, E.L. Thomas, A Dielectric Omnidirectional Reflector. Science **282**, 1679–1682 (1998)
82. Y. Fink, D.J. Ripin, S. Fan, C. Chen, J.D. Joannopoulos, E.L. Thomas, Guiding optical light in air using an all-dielectric structure. J. Lightwave Technol. **17**(11), 2039–2041 (1999)
83. P. Yeh, A. Yariv, E. Marom, Theory of bragg fiber. J. Opt. Soc. Am. **68**, 1196–1201 (1978)
84. S. Johnson, M. Ibanescu, M. Skorobogatiy, O. Weisberg, T. Engeness, M. Soljacic, S. Jacobs, J. Joannopoulos, Y. Fink, Low-loss asymptotically single-mode propagation in large-core omniguide fibers. Opt. Express **9**(13), 748–779 (2001)
85. M. Ibanescu, S.G. Johnson, M. Soljacic, J.D. Joannopoulos, Y. Fink, Analysis of mode structure in hollow dielectric waveguide fibers. Phys. Rev. E **67**, 046608 (2003)
86. O. Shapira, A.F. Abouraddy, J.D. Joannopoulos, Y. Fink, Complete modal decomposition for optical waveguides. Phys. Rev. Lett. **94**, 143902 (2005)
87. O. Shapira, A.F. Abouraddy, Q. Hu, D. Shemuly, J.D. Joannopoulos, Y. Fink, Enabling coherent superpositions of iso-frequency optical states in multimode fibers. Opt. Express **18**(12), 12622–12629 (2010)
88. D. Shemuly, Z.M. Ruff, A.M. Stolyarov, G. Spektor, S.G. Johnson, Y. Fink, O. Shapira, Asymmetric wave propagation in planar chiral fibers, **21**(2), 1465–1472 (2012)
89. http://www.omni-guide.com/
90. A. Yildirim, M. Vural, M. Yaman, M. Bayindir, Bioinspired optoelectronic nose with nanostructured wavelength-scalable hollow-core infrared fibers. Adv. Mat. **23**, 1263–1267 (2011)

91. H. Qu, M. Skorobogatiya, Liquid-core low-refractive-index-contrast bragg fiber sensor. Appl. Phys. Lett. **98**, 201114 (2011)

92. K.J. Rowland, S. Afshar, A. Stolyarov, Y. Fink, T.M. Monro, Bragg waveguides with low-index liquid cores. Opt. Express **20**(1), 48–62 (2012)

93. O. Shapira, K. Kuriki, N.D. Orf, A.F. Abouraddy, G. Benoit, J.F. Viens, A. Rodriguez, M. Ibanescu, J.D. Joannopoulos, Y. Fink, M.M. Brewster, Surface-emitting fiber lasers. Opt. Express **14**(9), 3929–3935 (2006)

94. S.D. Hart, G.R. Maskaly, B. Temelkuran, P.H. Prideaux, J.D. Joannopoulos, External reflection from omnidirectional dielectric mirror fibers. Science **296**, 510–513 (2002)

95. G. Benoit, S.D. Hart, B. Temelkuran, J.D. Joannopoulos, Y. Fink, Static and dynamic properties of optical microcavities in photonic bandgap yarns. Adv. Mater. **15**(24), 2053–2056 (2003)

96. G. Benoit, K. Kuriki, J.F. Viens, J.D. Joannopoulos, Y. Fink, Dynamic all-optical tuning of transverse resonant cavity modes in photonic bandgap fibers. Opt. Lett. **30**(13), 1620–1622 (2005)

97. F. Sorin, G. Lestoquoy, S. Danto, J.D. Joannopoulos, Y. Fink, Resolving optical illumination distributions along an axially symmetric photodetecting fiber. Opt. Express **18**(23), 24264–24275 (2010)

98. A. Gumennik, A.M. Stolyarov, B. Schell, C. Hou, G. Lestoquoy, F. Sorin, W. McDaniel, A. Rose, J.D. Joannopoulos, Y. Fink, All-in-fiber chemical sensing. Adv. Mater. adma201203053 (in press, 2012)

99. S. Danto, F. Sorin, N.D. Orf, Z. Weng, S.A. Speakman, J.D. Joannopoulos, Y. Fink, Fiber field-effect device via in situ channel crystallization. Adv. Mater. **22**, 4162–4166 (2010)

100. S. Danto, Z. Ruff, Z. Wang, J.D. Joannopoulos, Y. Fink, Ovonic memory switching in multimaterial fibers. Adv. Funct. Mat. **21**(6), 1095–1101 (2011)

101. R.M. Wood, S.K. Sharam, P. Waite, in *Variation of Laser Induced Damage Threshold with Laser Pulse Repetition Frequency, Laser Induced Damage in Optical Material*, *1982*. Ed. by H.E. Bennett, A.H. Guenther, D. Milam, B.E. Newnam, Proceedings of a symposium sponsored by National Bureau of Standards, Boulder, Colorado, 44–49, 1984

102. B.M. Cowan, in *Optical Damage Threshold of Silicon for Ultrafast Infrared Pulses, Laser-Induced Damage in Optical Materials: 2007*. ed by G.J. Exarhos, A.H. Guenther, K.L. Lewis, D. Ristau, M.J Soileau, C.J Stolz, Proceedings of the SPIE, 6720, 67201 M, 2008

103. B. Jalali, V. Raghunathan, D. Dimitropoulos, O. Boyraz, Raman-based silicon photonics. IEEE J. Sel. Top. Quantum Electron. **12**(3), 412–421 (2006)

104. V. Raghunathan, D. Borlaug, R. Rice, B. Jalali, Demonstration of a mid-infrared silicon raman amplifier. Opt. Express **15**, 14355–14362 (2007)

105. M. Lipson, Guiding, modulating, and emitting light on silicon—challenges and opportunities. J. Lightwave Technol. **23**(12), 4222–4238 (2005)

106. G.T. Reed, A.P. Knights, *Silicon Photonics: An Introduction* (wiley, Chichester, 2004)

107. J. Leuthold, C. Koos, W. Freude, Nonlinear silicon photonics. Nat. Photonics **4**, 535–544 (2010)

108. J. Michel, J. Liu, L.C. Kimerling, High-performance ge-on-si photodetectors. Nat. Photonics **4**, 527–534 (2010)

109. J. Ballato, T. Hawkins, P. Foy, B. Yazgan-Kokuoz, R. Stolen, C. McMillen, N.K. Hon, B. Jalali, R. Rice, Glass-clad single-crystal germanium optical fiber. Opt. Express **17**(10), 8029–8035 (2009)

110. C. McMillen, T. Hawkins, P. Foy, D. Mulwee, J. Kolis, R. Stolen, R. Rice, J. Ballato, On crystallographic orientation in crystal core optical fibers. Opt. Mater. **32**(9), 862–867 (2010)

111. J. Ballato, T. Hawkins, P. Foy, C. McMillen, L. Burka, J. Reppert, R. Podila, A. Rao, R. Rice, Binary iii–v core semiconductor optical fiber. Opt. Express **18**(5), 4972–4979 (2009)

112. P. Dragic, T. Hawkins, P. Foy, S. Morris, J. Ballato, Sapphire-derived all-glass optical fibres. Nat. Photonics **6**, 627–633 (2012)

113. S. Morris, C. McMillen, T. Hawkins, P. Foy, R. Stolen, J. Ballato, R. Rice, The influence of core geometry on the crystallography of silicon optical fiber. J. Cryst. Growth **352**(1), 53–58 (2011)
114. N. Gupta, C. McMillen, R. Singh, R. Podila, A.M. Rao, T. Hawkins, P. Foy, S. Morris, R. Rice, K.F. Poole, L. Zhu, J. Ballato, Annealing of silicon optical fibers. J. Appl. Phys. **110**, 093107 (2011)
115. S. Morris, T. Hawkins, P. Foy, C. McMillen, J. Fan, L. Zhu, R. Stolen, R. Rice, J. Ballato, Reactive molten core fabrication of silicon optical fiber. Opt. Mater. Express **1**(6), 1141–1149 (2011)
116. B.R. Jackson, P.J.A. Sazio, J.V. Badding, Single-crystal semiconductor wires intetrated into microstructured optical fibers. Adv. Mat. **20**, 1135–1140 (2008)
117. J.R. Sparks, R. He, N. Healy, M. Krishnamurthi, A.C. Peacock, P.J.A. Sazio, V. Gopalan, J.V. Badding, Zinc selenide optical fibers. Adv. Mat. **23**, 1647–1651 (2011)
118. D.M. Dobkin, M.K. Zuraw (eds.), *Principles of Chemical Vapor Deposition* (Kluwer, Dordrecht, 2003)
119. R. He, P.J.A. Sazio, A.C. Peacock, N. Healy, J.R. Sparks, M. Krishnamurthi, V. Gopalan, J.V. Badding, Integration of gigahertz-bandwidth semiconductor devices inside microstructured optical fibres. Nat. Photonics **6**, 174–179 (2012)
120. D.-J. Won, M.O. Ramirez, H. Kang, V. Gopalan, N.F. Baril, J. Calkins, J.V. Badding, P.J.A. Sazio, All-optical modulation of laser light in amorphous silicon-filled microstructured optical fibers. Appl. Phys. Lett. **91**, 161112 (2007)
121. C.E. Finlayson, A. Amezcua-Correa, P.J.A. Sazio, N.F. Baril, J.V. Badding, Electrical and raman characterization of silicon and germanium-filled microstructed optical fibers. Appl. Phys. Lett. **90**, 132110 (2007)
122. A. Tuniz, B.T. Kuhlmey, R. Lwin, A. Wang, J. Anthony, R. Leonhardt, S.C. Fleming, Drawn metamaterials with plasmonic response at terahertz frequencies. Appl. Phys. Lett. **96**, 191101 (2010)
123. E.J. Smith, Z. Liu, Y. Mei, O.G. Schmidt, Combined surface plasmon and classical waveguiding through metamaterial fiber design. Nano Lett. **10**, 1–5 (2010)
124. A. Wang, A. Tuniz, P.G. Hunt, E.M. Pogson, R.A. Lewis, A. Bendavid, S.C. Fleming, B.T. Kuhlmey, M.C.J. Large, Fiber metamaterials with negative magnetic permeability in the terahertz. Opt. Mater. Express **1**(1), 115–120 (2011)
125. A. Tuniz, R. Lwin, A. Argyros, S.C. Fleming, E.M. Pogson, E. Constable, R.A. Lewis, B.T. Kuhlmey, Stacked-and-drawn metamaterials with magnetic resonances in the terahertz range. Opt. Express **19**(17), 16480–16490 (2011)
126. A. Tuniz, B. Pope, A. Wang, M.C.J. Large, S. Atakaramians, S.-S. Min, E.M. Pogson, R.A. Lewis, A. Bendavid, A. Argyros, S.C. Fleming, B.T. Kuhlmey, Spatial dispersion in three-dimensional drawn magnetic metamaterials. Opt. Express **20**(11), 11924–11935 (2012)
127. R.C. McPhedran, I.V. Shadrivov, B.T. Kuhlmey, Y.S. Kivsha, Metamaterials and metaoptics. NPG Asia Mater. **3**, 100–108 (2011)
128. H.K. Tyagi, H.W. Lee, P. Uebel, M.A. Schmidt, N. Joly, M. Scharrer, P.St.J. Russell, Plasmon resonances on gold nanowires directly drawn in a step-index fiber. Opt. Lett. **35**(15) 2573–2575 (2010)
129. J. Hou, D. Bird, A. George, S. Maier, B.T. Kuhlmey, J.C. Knight, Metallic mode confinement in microstructured fibres. Opt. Express **16**(9), 5983–5990 (2008)
130. C.G. Poulton, M.A. Schmidt, G.J. Pearce, G. Kakarantzas, P.St.J. Russell, Numerical study of guided modes in arrays of metallic nanowires, Opt. Lett. **32**(12), 1647–1649 (2007)
131. M.A. Schmidt, L.N.P. Sempere, H.K. Tyagi, C.G. Poulton, P.St.J. Russell, Waveguiding and plasmon resonances in two-dimensional photonic lattices of gold and silver nanowires. Phys. Rev. B **77**, 033417 (2008)
132. H.W. Lee, M.A. Schmidt, H.K. Tyagi, L.N. Prill Sempere, P.St.J. Russell, Polarization-dependent coupling to plasmon modes on submicron gold wire in photonic crystal fiber, Appl. Phys. Lett. **93**(11), 111102 (2008)

133. H.W. Lee, M.A. Schmidt, R.F. Russell, N.Y. Joly, H.K. Tyagi, P. Uebel, P.St.J. Russell, Pressure-assisted melt-filling and optical characterization of au nano-wires in microstructured fibers, Opt. Express **19**(13), 12180–12189 (2011)
134. S. Shabahang, M.P. Marquez, G. Tao, J.J. Kaufman, M.U. Piracha, D. Nguyen, P.J. Delfyett, A.F. Abouraddy, Octave-spanning infrared supercontinuum generation in robust chalcogenide fiber nano-tapers using picosecond pulses. Opt. Lett. **37**(22), 4639–4641 (2012)
135. S. Shabahang, G. Tao, J.J Kaufman, A.F. Abouraddy, Dispersion characterization of chalcogenide bulk glass, composite fibers, and robust nano-tapers, J. Opt. Soc. Am. B, in press (2012)
136. N. Granzow, S.P. Stark, M.A. Schmidt, A.S. Tverjanovich, L. Wondraczek, P.St.J. Russell, Supercontinuum generation in chalcogenide-silica step-index fibers. Opt. Express **19**(21), 21003–21010 (2011)
137. N. Granzow, P. Uebel, M.A. Schmidt, A.S. Tverjanovich, L. Wondraczek, P.St.J. Russell, Bandgap guidance in hybrid chalcogenide–silica photonic crystal fibers. Opt. Lett. **36**(13), 2432–2434 (2011)
138. A. Gumennik, L. Wei, G. Lestoquoy, A.M. Stolyarov, X. Jia, P.H. Rekemeyer, M.J. Smith, X. Liang, S.G. Johnson, S. Gradečak, A.F. Abouraddy, J.D. Joannopoulos, Y. Fink, Silicon-in-Silica spheres via axial thermal gradient in-fibre capillary instabilities. Nat. Commun. **4**, 2216 (2013). doi:10.1038/ncomms3216